International Journal of Advanced Engineering and Technology Research
ISSN: 3106-8677 (Print), ISSN: 3106-8685 (Online) | Vol. 1, No. 2, 2026

Study on the Influence of Anti-Slip Pile on the Mechanical Response of Pipeline Under Landslide

Hao Liu [1], Bangwen Fu [2], Jiaxin Jia [3]

[1] School of Mechanical and Electrical Engineering, Southwest Petroleum University, Chengdu 610500, China

[2] Engineering Quality Supervision and Inspection Co., Ltd., National Pipe Network Group, Beijing 100000, China

[3] Sichuan Highway and Bridge Construction Group Co., Ltd., Chengdu 610041, China

[*] **Corresponding author**: Guang Yao

Abstract: In the process of laying anti-slip piles, by adjusting their number, spacing, shape, size and other parameters to analyze the changes of landslide morphology and pipeline stress under different working conditions, the reinforcement effect can be optimized and provide a basis for landslide control in actual engineering. Based on the strength reduction method, the finite element software ABAQUS was used to establish a numerical model of the sliding slope impact gas pipeline under the reinforcement effect of anti-slip pile, realize the pile-soil interaction analysis, and study the mechanical response of the gas pipeline under different reinforcement methods. The results show that when the number of anti-slip piles increases, the overall displacement of the sliding body decreases, and for the gas pipeline, the displacement decreases with the increase of the number of anti-slip piles, and the decrease range reaches 168.1mm, a year-on-year decrease of 35.89%, while the maximum effective stress of the pipeline increases first and then decreases with the increase of the number of anti-slip piles. When the size of the anti-slip pile increases, the maximum displacement of the sliding body gradually decreases, and the anti-slip effect of the soil directly above the slip pile and at the perimeter of the landslide slope is particularly obvious, indicating that the anti-slip pile size increases significantly to enhance its anti-slip effect on the slope. Although the construction of cylindrical anti-slip pile is smaller than that of square anti-slip pile, its anti-slip ability to resist slope is worse and its own anti-deformation ability is weaker.

Keywords: Landslide, anti-slip piles, landslide management, strength reduction method, pile soil interaction.

1. Introduction

The structural design of anti-slide piles has now reached a highly mature stage. The primary steps involve determining the magnitude of landslide impact forces, analyzing stress and displacement distributions within the landslide mass, estimating the stress levels on anti-slide piles based on these analyses, selecting appropriate materials and dimensions, and optimizing pile placement strategies within slope structures. Numerical simulations enable comprehensive evaluation of anti-slide pile effectiveness under various operational conditions. Comparative analyses of piles with different dimensions and geometries provide critical design references, while simulations examining spacing configurations enhance spatial layout optimization for improved landslide resistance. Studies on soil displacement patterns and pipeline stress distribution deepen understanding of pile-soil interaction mechanisms, offering theoretical foundations for safe pipeline operations through landslide zones. Extensive research has been conducted on anti-slide pile mechanisms [1]. Zeng Jinxiu [2] employed theoretical analysis, numerical modeling, and laboratory experiments to study reinforced slopes using two typical engineering cases, elucidating the mechanisms of composite anti-slide pile reinforcement and developing analytical methods for micro-pile composite structures. Huang Yongjin [3] utilized theoretical modeling and numerical simulations to investigate pressure distribution patterns in soil-rock composite slopes under pile loading, analyzing dynamic stress variations in pile bodies and soil-rock masses during landslide progression. Comparative validation with full-scale tests confirmed the reliability of these methodologies. Wang Long et al. [4] investigated the impact of anti-slide pile arrangement methods on slope reinforcement effectiveness. The results demonstrated that slope reinforcement efficacy correlates significantly with anti-slide pile location, spacing, and soil friction angle. Optimal reinforcement effects were achieved when anti-slide piles were positioned in the upper-middle slope section with a pile spacing-to-diameter ratio of 4. Li Ming [5] employed the strength reduction method and ABAQUS software to establish contact models between anti-slide piles and landslide masses, calculating sliding resistance effects under varying pile lengths and diameters. These findings provide reference insights for landslide control and buried pipeline protection. Wu et al. [6] proposed an efficient new type of retaining wall-style anti-slide pile that modifies traditional cantilever stress states and relies on lateral foundation reaction forces to balance landslide thrust, deriving theoretical calculation formulas. Lian et al. [7] utilized 3D numerical simulation software FLAC3D to develop engineering-based numerical models incorporating pile-soil contact element properties, analyzing anti-slide pile effects and pile-soil interactions. Comparative analysis of model-induced slip zone displacements with field observation data validated the model's reliability. Fan et al. [8] conducted large-scale vibration table tests to study dynamic responses of double-row anti-slide piles and prestressed anchor cable reinforced slopes. Experimental results revealed that lateral soil pressure peaks behind anti-slide piles at slope bases significantly exceeded those behind piles at slope flanks. Zhang et al. [9] employed a combined approach of model testing and numerical simulation to analyze the evolution mechanism and influencing parameters of soil arch effects in anchored anti-slide piles from both qualitative and

quantitative perspectives. The results demonstrated that during the formation and development of soil arches, soil particles between piles transmit landslide thrust to anti-slide piles through these arch structures. The load-bearing capacity of soil arches decreases with increasing pile spacing, while enhanced soil compaction significantly improves their load-bearing capability, thereby maximizing their anti-slide performance. Literature review on anti-slide pile effects reveals that as specialized lateral load-bearing piles, they can transfer landslide forces to stable strata through mutual interaction with surrounding geotechnical materials, utilizing the anchoring action and passive resistance of stabilized strata to counteract sliding forces. Numerical simulations under various operational conditions revealed strong correlations between slope reinforcement effectiveness and factors including pile location, spacing, and soil friction angle. Optimal reinforcement outcomes were achieved when anti-slide piles were positioned in the upper-middle slope section with a pile spacing-to-diameter ratio of 4.

Previous studies have comprehensively summarized analytical methods for landslide reinforcement using anti-slide piles, which can be simply categorized into the following three types:

(1) The displacement method is a widely adopted approach for analyzing soil slopes reinforced with anti-slide piles, typically calculating pile displacements and stress-strain responses based on pile-soil interaction. Building upon the elastic foundation beam model, this method incorporates pile-soil interaction by first establishing differential equations for the pile's deflection curve, then assuming displacement during slope sliding, and finally solving them through iterative calculations [10].

(2) The pressure method can also be applied to theoretical analysis of landslide reinforcement using anti-slide piles. When applying this method for pile design, the pile body above the sliding surface is treated as a free end subjected to known sliding thrust, while the pile body below the sliding surface is fixed in stable deep soil and rock. This approach resembles the cantilever pile method used in cantilever structures.

(3) As an advanced computer-aided method, the finite element method [11] has been widely applied in recent years to analyze anti-slide pile reinforcement for landslides. Leveraging the advantages of finite element simulation software—such as user-friendly operation, short processing time, and low cost—we conducted calculations on various landslide models under different conditions by adjusting model parameters. The resulting stress-strain data of buried pipelines were systematically analyzed and compared, ultimately optimizing the parameters of anti-slide piles to protect buried pipelines.

2. Finite Element Model for Slope Reinforcement Using Anti-slide Piles

To investigate the effectiveness of anti-slide piles in slope stabilization for pipeline protection under various operating conditions, this study employed the finite element software ABAQUS to establish a model for slope reinforcement with anti-slide piles. Considering the excessive computational load, a semi-model approach was adopted. The Mohr-Coulomb soil constitutive model was utilized for soil behavior simulation. To ensure simulation results align closely with practical conditions, the strength reduction method was maintained for modeling soil slip processes, with calculations terminated upon convergence failure. Contact interactions were categorized into two types: normal contact (implemented using a "hard contact" model) and tangential contact (implemented using frictional contact models). The pipeline specifications include an inner diameter of 1016 mm and wall thickness of 20 mm. Anti-slide pile parameters were determined in accordance with guidelines from the "Geological Disaster Prevention and Monitoring Technology for Oil and Gas Pipelines" [12]. Material parameters for both pipelines and soil are listed in Table 1. Anti-slide piles were installed 3 meters upstream of pipelines, featuring square cross-sections with 0.9-meter side lengths and 8.3-meter burial depths. Spacing between piles was maintained at 3.5 meters, with detailed layout configurations and dimensional parameters illustrated in Figure 1.

Table 1. Pipe and soil material parameters

material	Density (kg/m3)	Elastic modulus (GPa)	Poisson ratio	yield strength (MPa)	Tensile strength (MPa)
X80 pipeline steel	7800	210	0.3	555	655
soil type	Density (kg/m3)	Elastic modulus (MPa)	Poisson ratio	angle of friction (°)	Cohesion (kPa)
soil mass in landslide area	2000	100	0.35	change with the variable	change with the variable
non-slide zone soil mass	2350	200	0.25	25	30

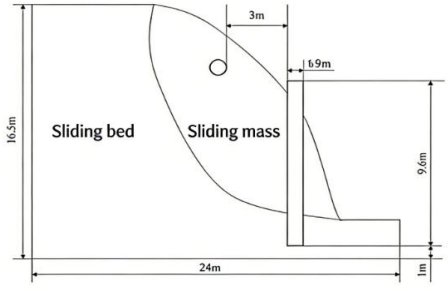

(a) Side view

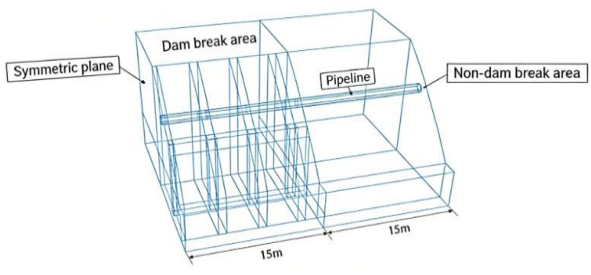

(b) Oblique view

Figure 1. Location and dimensional parameters of anti-slip pile (half model)

In practical engineering applications, anti-slide piles used

for landslide control are typically constructed with C30 concrete. The material parameters of these piles in this simulation are presented in Table 2.

Table 2. Material parameters of anti-slip pile

Anti-slide pile material	Density (kg/m^3)	elastic modulus (MPa)	Poisson ratio
C30 concrete	2400	3×104	0.2

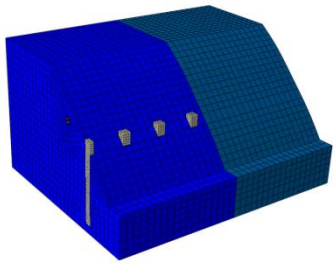

(a) Model mesh

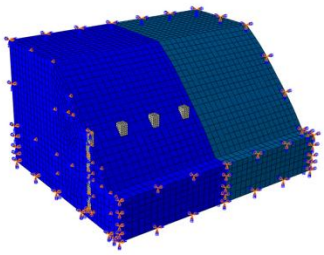

(b) Model boundary conditions

Figure 2. Schematic diagram of the reinforced slope grid of anti-slip piles

Prior to computation, the model requires meshing of its components, as illustrated in Figure 2. The assembly consists of three primary elements: soil, anti-slide piles, and pipelines. Specifically, orange grids represent pipelines, blue grids denote landslide zone soil, light blue grids indicate non-slide zone soil, and white grids correspond to anti-slide piles. All grids employ C3D8R hexahedral elements, totaling 25,671 grids and 33,304 nodes. To ensure computational accuracy, pipeline grids and adjacent areas are mesh-enclosed. The contact between anti-slide piles and soil is defined as "hard contact" with a friction coefficient of 0.5. Boundary conditions are configured as follows: left and right sides are z-axis symmetric, the landslide base and front face are fully constrained, while the rear side retains only vertical displacement. Anti-slide piles are fixed in the model.

3. Influence of the Number of Anti-slip Piles on the Pipe Stress

In landslide prevention and control processes, the number of anti-slide piles is a key concern for engineering professionals. The quantity of anti-slide piles in soil not only affects construction costs but also impacts landslide mitigation effectiveness. To investigate the influence of anti-slide pile quantity on buried gas pipelines, this section designed five operational scenarios with detailed parameters shown in Table 3. All parameters remained consistent except for the varying anti-slide pile counts.

Table 3. Parameters of anti-slip piles under each working condition

order number	Anti-slide pile material	Number of anti-slide piles	spacing of anti-slide piles	dimension of anti-slide pile
Comparison protocol	No concrete	0	not have	not have
Option 1	C30 concrete	1	3.5m	0.9m×0.9m×9.6m
Option 2	C30 concrete	2	3.5m	0.9m×0.9m×9.6m
Option 3	C30 concrete	3	3.5m	0.9m×0.9m×9.6m
Option 4	C30 concrete	4	3.5m	0.9m×0.9m×9.6m

Figure 3 presents displacement cloud diagrams of soil mass under varying numbers of anti-slide piles. The data clearly demonstrates that soil displacement is significantly influenced by pile placement. In the absence of anti-slide piles, substantial displacement occurs primarily at the landslide center (model symmetry plane), with displacement values decreasing progressively from the center toward the periphery. As the number of anti-slide piles increases, overall soil displacement decreases, and the maximum displacement zone gradually shifts from the center to the perimeter, ultimately reaching directly above the piles. This progression indicates that higher pile density yields superior landslide stabilization effects.

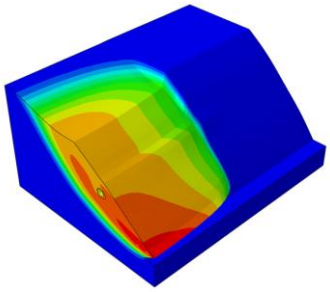

(a) Comparison programmes

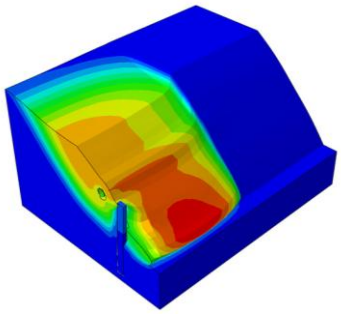

(b) Programme I

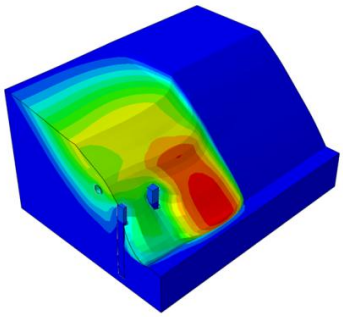

(c) Programme II

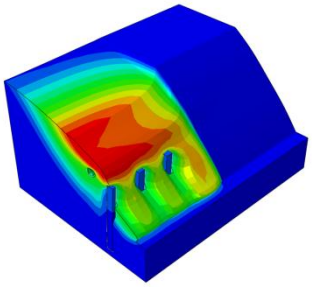

(d) Programme III

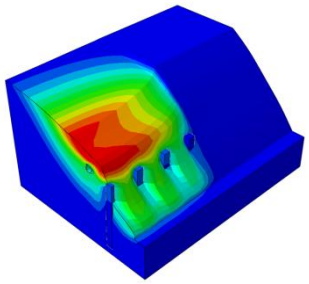

(e) Programme IV

Figure 3. Soil displacement cloud diagram of sliding slope under different working conditions

To maintain consistent simulation duration, the results are presented in the following charts. Table 4 summarizes the maximum Von Mises stress, maximum displacement, and axial strain experienced by the pipeline under various operating conditions. Figure 5-3 displays the stress cloud maps of the pipeline with different numbers of anti-slide piles, while Figure 4 illustrates the variation relationship between maximum displacement and axial displacement under different operating conditions.

Table 4. Table of force deformation of pipelines under different working conditions

order number	Maximum pipe displacement (mm)	Maximum Von Mises stress in the pipe (MPa)	Maximum axial strain of the pipe (%)	Degree of damage
Comparison protocol	468.4	572.4	0.256	plastic deformation
Option 1	419.2	615.3	0.231	plastic deformation
Option 2	341.2	564.3	0.191	plastic deformation
Option 3	319.9	559	0.19	plastic deformation
Option 4	300.3	455.4	0.17	elastic bending

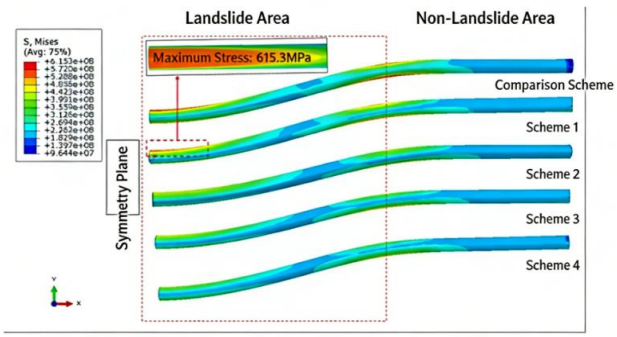

Figure 4. Pipe stress cloud under different working conditions

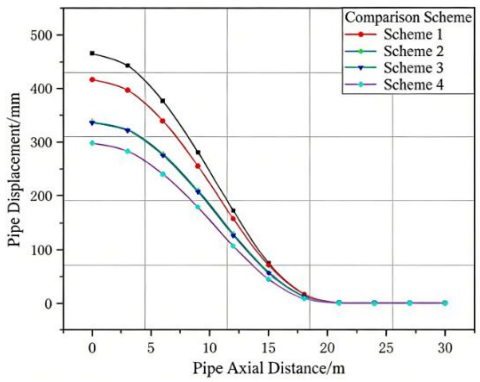

Figure 5. Diagram of pipe displacement along axial direction under different working conditions

The results quantitatively demonstrate the impact of anti-slide pile quantity on pipeline stress distribution. Overall,

axial strain values showed minimal variation across five design schemes, indicating limited influence of pile count on gas pipeline deformation. Pipeline displacement decreased with increasing axial distance from ground level, with segments located at landslide center zones (symmetrical planes) exhibiting maximum displacement and highest failure risk. Without anti-slide pile reinforcement, pipelines experienced significant deformation reaching 468.4mm maximum displacement and 572.4MPa peak effective stress exceeding material yield limits, posing failure risks. When using single anti-slide piles, maximum effective stress increased compared to control schemes due to insufficient sliding resistance and soil flow redirection causing lateral soil accumulation, resulting in 615.3MPa stress levels. Further pile deployment achieved substantial reductions in both maximum displacement and stress (up to 18.6% decrease), confirming effective anti-slide functionality. While Scheme 2 and 3 maintained stress levels slightly above material yield limits, Scheme 4 demonstrated stress values below these thresholds, transitioning from plastic to elastic deformation. These findings indicate enhanced landslide stabilization effects and improved pipeline safety with increased pile density. Practical engineering should prioritize optimal pile deployment within budget constraints to ensure stable pipeline operation.

4. Influence of the Size of Anti-Slip Pile on the Pipe Stress

In landslide control engineering, both the quantity and dimensions of anti-slide piles significantly impact treatment effectiveness. These piles are typically deployed in mountainous regions with complex geological conditions, where their size not only determines reinforcement efficacy but also influences construction volume and costs. This study focuses on selecting optimal anti-slide pile dimensions to minimize engineering requirements while ensuring stabilization outcomes. To investigate the effects of varying pile dimensions on pipeline stress distribution, three design schemes were developed alongside a numerical model without anti-slide piles as control group, totaling four configurations. All variables except pile dimensions remained constant (see Table 5 for specific parameters). Through numerical simulations of gas pipelines under different operational conditions, comprehensive analytical results were obtained.

Table 5. Anti-slip pile parameter table under each working condition

order number	Anti-slide pile material	Number of anti-slide piles	spacing of anti-slide piles	dimension of anti-slide pile
Comparison protocol	No concrete	0	not have	not have
Option 1	C30 concrete	3	3.5m	0.9m×0.9m×9.6m
Option 2	C30 concrete	3	3.5m	1.4m×1.4m×9.6m
Option 3	C30 concrete	3	3.5m	1.9m×1.9m×9.6m

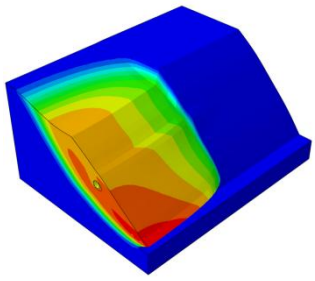

(a) Comparison programmes

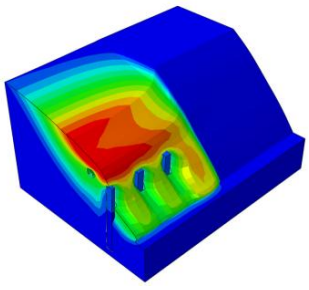

(b) Programme I

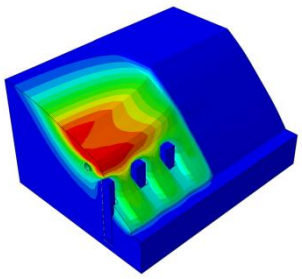

(c) Programme II

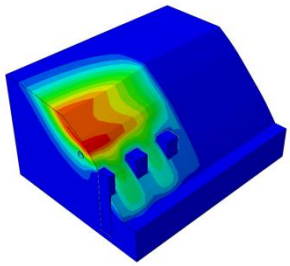

(d) Programme III

Figure 6. Soil displacement cloud of sliding slope under different working conditions

Figure 6 presents displacement cloud diagrams of landslide soil under varying anti-slide pile dimensions. The analysis qualitatively demonstrates the impact of pile size on landslide stabilization effects. Without anti-slide piles, the landslide exhibits significant overall displacement with soil accumulation concentrated at the central model symmetry plane, where displacement values progressively decrease toward the periphery. The presence of anti-slide piles

substantially reduces displacement, with maximum displacement concentrated directly above the piles. As pile dimensions increase, maximum displacement gradually diminishes, particularly at the landslide periphery. These findings indicate that larger anti-slide pile dimensions significantly enhance stabilization performance, with particularly pronounced effects observed at both the periphery and directly above the piles.

To maintain consistent simulation duration, we conducted stress analysis of gas transmission pipelines under various operating conditions. The following charts illustrate the stress distribution characteristics under different scenarios. Table 6 presents maximum effective stress and displacement values for gas pipelines with varying anti-slide pile dimensions, while Figure 7 displays Von Mises stress cloud diagrams corresponding to different pile sizes. Figure 8 further illustrates the axial displacement variation patterns along the pipeline axis.

Table 6. Table of force deformation of gas pipeline under different working conditions

order number	Maximum pipe displacement (mm)	Maximum Von Mises stress in the pipe (MPa)	Maximum axial strain of the pipe (%)	Degree of damage
Comparison protocol	468.4	572.4	0.256	plastic deformation
Option 1	319.9	559	0.19	plastic deformation
Option 2	301.2	475.4	0.164	elastic bending
Option 3	232.9	464.7	0.138	elastic bending

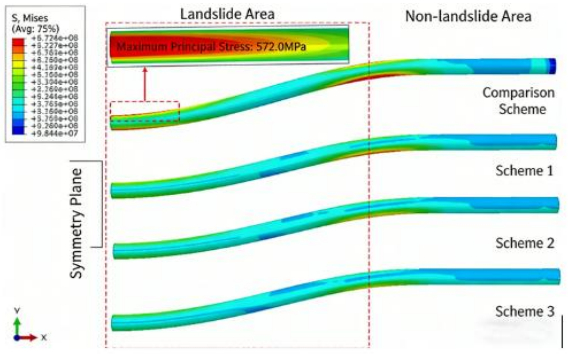

Figure 7. Stress cloud diagram of gas pipeline under different working conditions

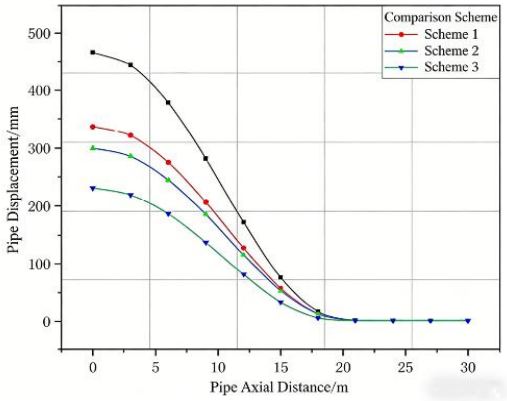

Figure 8. Diagram of pipe displacement along axial direction under different working conditions

The above charts enable quantitative analysis of gas pipeline stress conditions under various operating scenarios. Overall, axial strain values show minimal variation across all four conditions, indicating negligible influence from anti-slide pile dimensions on pipeline deformation. Pipeline displacement exhibits a decreasing trend along the axial direction, with maximum displacement occurring at landslide center (model symmetry plane) and progressively decreasing toward the landslide boundary—a characteristic determined by soil accumulation volume. In scenarios without anti-slide piles, both effective stress and displacement remain elevated, with peak effective stress exceeding material yield limits and triggering plastic deformation. The presence of anti-slide piles significantly reduces effective stress and displacement, though maximum effective stress still reaches 559MPa, surpassing yield thresholds and inducing plastic deformation. Notably, maximum effective stress demonstrates pronounced reduction with increasing pile dimensions: in Scenario 2 and Scenario 3, stress levels drop below material yield limits, indicating elastic bending behavior. Crucially, the stress reduction effect becomes more pronounced when pile cross-sections expand from 0.9m×0.9m to 1.4m×1.4m compared to 1.4m×1.4m to 1.9m×1.9m, demonstrating significant marginal benefits in enhanced pipeline protection capacity through dimensional scaling. In conclusion, increasing the size of anti-slide piles can enhance sliding resistance to some extent, but beyond a certain threshold, the improvement becomes negligible while significantly increasing construction workload and costs. Therefore, when selecting anti-slide piles, engineers should carefully balance project requirements and budgetary constraints, avoiding excessive size expansion.

5. Influence of Anti-slide Pile Shape on Pipeline Stress

Previous studies have examined how the quantity and dimensions of anti-slide piles affect the stress distribution in gas pipelines. Beyond these two factors, the shape of anti-slide piles also significantly influences pipeline stress behavior. Due to variations in construction methods, square-shaped anti-slide piles are commonly used in China, while cylindrical designs prevail in Europe and North America. To investigate the impact of different pile shapes on pipeline stress, this section presents two typical configurations: square and cylindrical anti-slide piles, along with a baseline scenario without anti-slide piles. All three configurations maintain identical parameters except for pile shape differences, as detailed in Table 7.

Table 7. Parameter table of anti-slip pile under each working condition

order number	Anti-slide pile material	Number of anti-slide piles	spacing of anti-slide piles	dimension of anti-slide pile
Comparison protocol	No concrete	0	not have	not have
Option 1	C30 concrete	4	3.5m	0.9m×0.9m×9.6m
Option 2	C30 concrete	4	3.5m	ϕ0.9m×9.6m

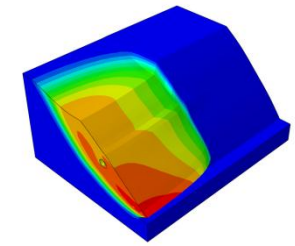

(a) Comparison programmes

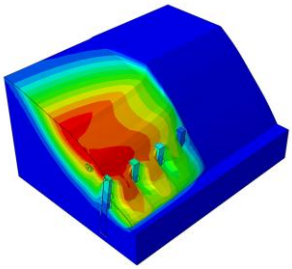

(b) Programme I

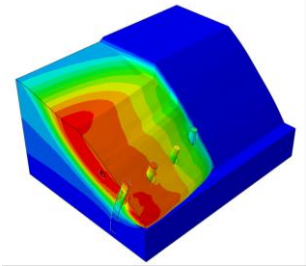

(c) Programme II

Figure 9. Soil displacement cloud of sliding slope under different working conditions

Figure 9 presents displacement cloud diagrams of landslide soils with different anti-slide pile configurations. The visual analysis clearly demonstrates the soil stabilization effects of anti-slide piles. In landslide scenarios without such supports, the absence of reinforcement leads to significant overall soil displacement, with high-displacement zones primarily concentrated at the landslide center (model symmetry plane). When anti-slide piles are embedded within the landslide mass, displacement values show substantial reduction, and high-displacement areas shift upward from the base toward the pile tops, predominantly distributed directly above the piles. Notably, transitioning from square to cylindrical anti-slide piles reduces their stabilizing efficacy, with displacement zones now distributed on both sides of the piles and increased bending deformation compared to square configurations. These findings indicate that pile geometry significantly impacts stabilization performance, with square anti-slide piles demonstrating superior stabilization effects and enhanced inherent deformation resistance compared to cylindrical counterparts.

To further investigate the impact of anti-slide pile geometry on gas pipeline stress under landslide conditions, stress and deformation analyses were conducted under varying operational scenarios with consistent simulation duration. Table 8 presents numerical values of pipeline stress and deformation under different conditions, Figure 10 displays stress cloud diagrams illustrating stress distribution patterns, while Figure 11 depicts axial displacement variation relationships across multiple operational scenarios.

Table 8. Pipe force deformation table under different working conditions

order number	Maximum pipe displacement (mm)	Maximum Von Mises stress in the pipe (MPa)	Maximum axial strain of the pipe (%)	Degree of damage
Comparison protocol	128.7	409.7	0.109	elastic bending
Option 1	86.5	350.2	0.0742	elastic bending
Option 2	91.7	364.5	0.0768	elastic bending

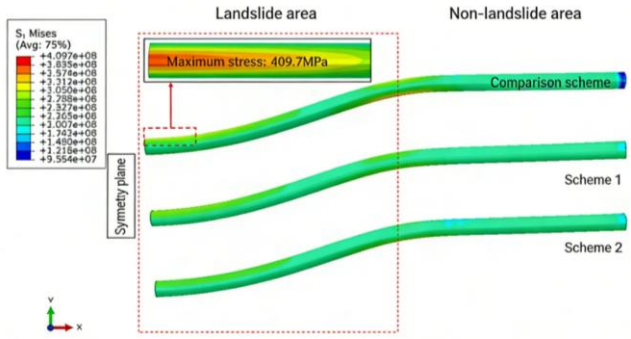

Figure 10. Effective stress cloud of gas pipeline under different working conditions

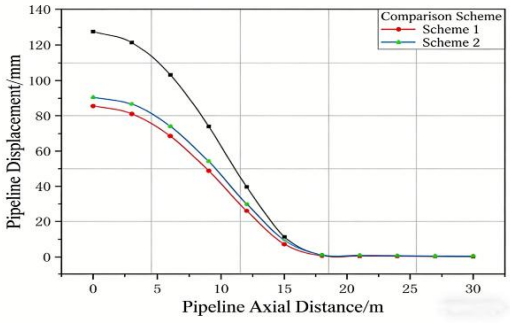

Figure 11. Diagram of pipe displacement along axial direction under different working conditions

The above charts provide quantitative analysis of stress-

deformation characteristics in gas pipelines under different anti-slide pile configurations. Overall, axial deformation patterns remain consistent with previous findings, exhibiting a gradual reduction trend along the longitudinal axis. During the simulation period, all three pipeline scenarios demonstrated plastic deformation, though stress and deformation values varied significantly. The comparative scheme exhibited markedly higher stress and deformation levels compared to the other two configurations, indicating that anti-slide piles of different geometries exert distinct anti-slide effects. Notably, Scheme 1 and Scheme 2 showed minimal differences in pipeline stress and deformation, with displacement variations of 5.2mm and effective stress differences of 14.3MPa. Scheme 1's pipeline stress-strain ratio slightly exceeded that of Scheme 2, suggesting that square anti-slide piles demonstrate slightly superior protective efficacy compared to cylindrical counterparts. Practical engineering applications should prioritize selecting appropriate pile geometries based on construction conditions and surrounding environmental factors.

6. Mechanical Response of Defective Pipelines under Anti-slip Piles

Previous studies have examined the mechanical response of intact pipelines under anti-slide pile reinforcement. However, in practical engineering applications, buried gas transmission pipelines are susceptible to adverse operating conditions such as third-party construction activities, rainwater erosion, and seismic events, which lead to the formation of various corrosion defects on both inner and outer walls. Building upon prior research, this chapter establishes a numerical model for reinforcing gas pipelines with internal corrosion defects subjected to slope impact under anti-slide pile conditions. The model dimensions remain consistent with previous studies, while corrosion defects are categorized into square and ellipsoidal shapes, as illustrated in Figure 12.

Referring to the above figure, further explanations are provided regarding the defect dimensions. For square corrosion defects, the length L is 60 mm, the width ω is 10°, and the depth D is 12 mm. For ellipsoidal corrosion defects, the length L, width ω, and depth D are consistent with those of square corrosion defects.

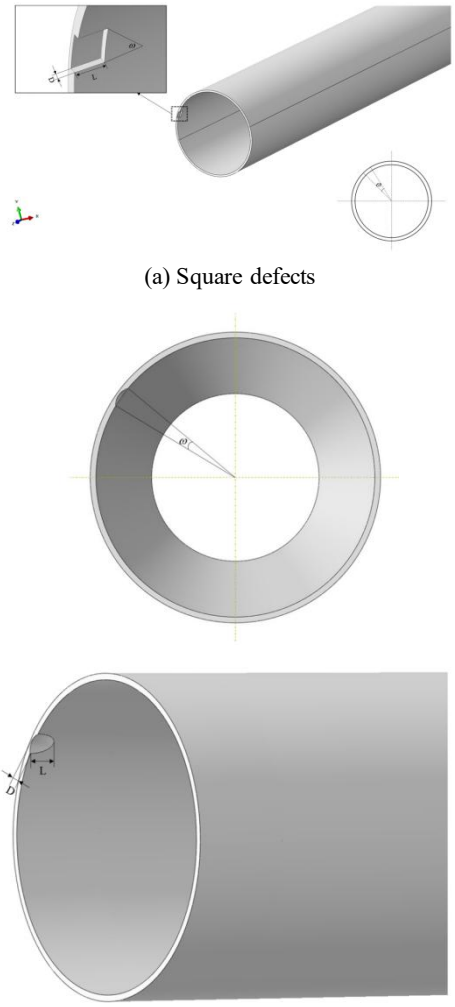

(a) Square defects

(b) Ellipsoidal defects

Figure 12. Schematic diagram of pipeline corrosion defects

To investigate the mechanical response of the pipeline with corrosion defects under the reinforcement of anti-slip piles, this chapter designs two working conditions: the pipeline with square defects and the pipeline with ellipsoidal defects. The numerical model without anti-slip pile protection is used as a comparison scheme. There are four working conditions in total, and the detailed parameters of each working condition are shown in Table 9.

Table 9. Model parameter table under each working condition

order number	Anti-slide pile material	Number of anti-slide piles	spacing of anti-slide piles	dimension of anti-slide pile	Defect shape
Compare Plan 1	No concrete	0	not have	not have	square
Compare Option Two	No concrete	0	not have	not have	spheroidicity
Option 1	C30 concrete	4	3.5m	0.9m×0.9m×9.6m	square
Option 2	C30 concrete	4	3.5m	0.9m×0.9m×9.6m	spheroidicity

To qualitatively analyze the influence of anti-slide piles on plastic deformation at pipeline defects, equivalent plastic strain cloud diagrams of gas pipelines under various operating conditions were generated, as shown in Figure 13.

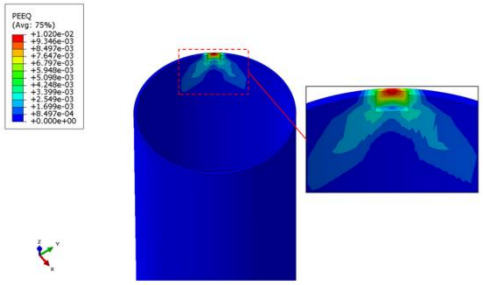

(a) Compare option one

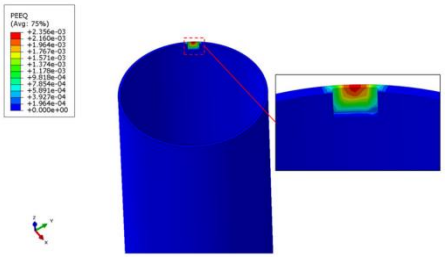

(b) Programme I

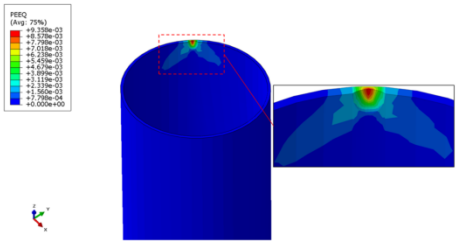

(c) Compare option two

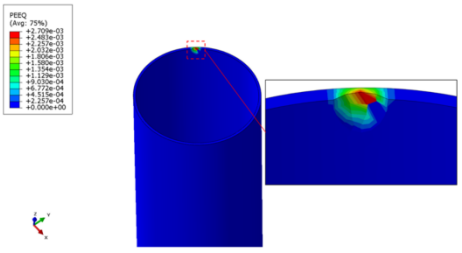

(d) Programme II

Figure 13. Equivalent plastic strain cloud diagram of pipeline under different working conditions

Analysis of the above cloud diagrams reveals that without anti-slide pile protection, the pipeline exhibits yielding behavior with equivalent plastic strain primarily concentrated near defects. The strain zone remains extensive, with maximum plastic strain occurring at the defect center and gradually decreasing as it extends outward. Both square and ellipsoidal defects demonstrate peak plastic strain at their centers, though square defects exhibit higher equivalent plastic strain peaks and broader high-strain zones compared to ellipsoidal defects. After implementing anti-slide pile reinforcement for slope stabilization, plastic deformation persists in the pipeline. Plastic strain zones near both defect types significantly diminish, with strain concentration shifting predominantly to internal defect regions. While maximum plastic strain remains consistent with pre-reinforcement levels at defect centers, equivalent strain peaks show substantial reduction. This indicates that anti-slide piles effectively limit plastic strain propagation near pipeline defects, mitigate structural damage severity, and provide protective benefits for gas pipelines traversing landslide-prone areas containing defects.

Based on the maximum displacement data of defective pipelines under various operating conditions, displacement peak curve diagrams for gas transmission pipelines at different time points were plotted, as shown in Figure 14.

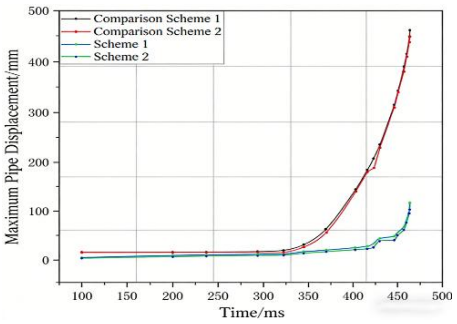

(a) Maximum displacement curve of pipeline under different working conditions

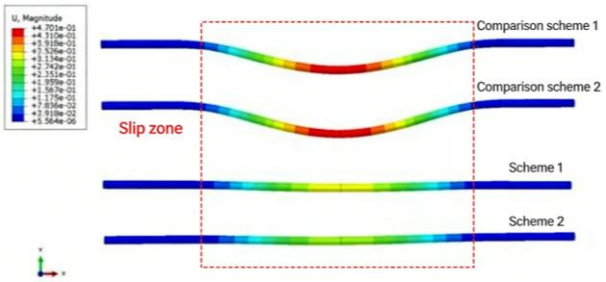

(b) Pipeline displacement cloud under different working conditions

Figure 14. contains the displacement curve and cloud plot of the defective pipeline

The figure above demonstrates that the displacement of defective gas pipelines exhibits nonlinear growth over time. When landslide impact duration ranges from 100ms to 340ms, pipeline displacement increases gradually. However, after exceeding 340ms, displacement rises significantly. This phenomenon occurs because landslide progression follows a slow initial phase during strength reduction method simulations, followed by abrupt acceleration after 340ms, causing rapid displacement under gravitational forces from overlying soil. Displacement values show minimal variation across pipelines with different defect geometries, indicating limited impact of defect shapes on peak displacement. Post-stabilization reinforcement using anti-slide piles reduces pipeline displacement by 74.5% (maximum reduction: 344.3mm) compared to un-stabilized conditions. The displacement peak-time curve demonstrates smoother dynamics than un-stabilized scenarios, confirming that anti-slide piles effectively mitigate landslide effects on defective pipelines and enhance operational stability for buried infrastructure.

To further investigate the cross-sectional stress conditions of defective pipelines after slope reinforcement with anti-slide piles, the cross-section of the gas transmission pipeline at the center of the sliding mass (model symmetry plane) at the same moment was selected, and the stress distribution diagram shown in Figure 15 was plotted.

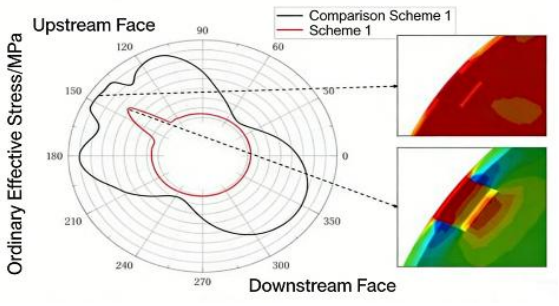

(a) Cross-sectional stress of pipelines with square defects

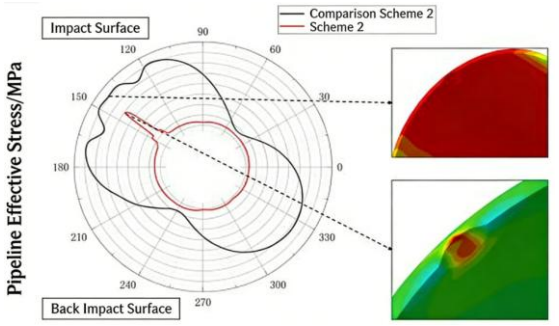

(b) Cross-sectional stress of pipes with ellipsoid defects

Figure 15. Cross-sectional stress of pipeline with defect under anti-slip pile reinforcement

The analysis of the figure reveals that under landslide impact, the cross-sectional stress distribution of pipelines at the landslide center exhibits symmetrical characteristics. High-stress zones are primarily concentrated on the impact-facing and impact-receiving surfaces, with significant stress concentration observed at defect locations. This indicates that corrosion defects severely compromise the load-bearing capacity of gas pipelines, posing threats to their safe and stable operation. When slope reinforcement with anti-slide piles is absent, the peak stress in pipelines with square defects reaches 562 MPa, exceeding the material yield limit and triggering plastic deformation. Pipelines with ellipsoidal defects demonstrate slightly lower peak stress values (555 MPa) compared to square defects. For regular-shaped defects studied in this research, stress values decrease progressively from the defect center outward, accompanied by pronounced equivalent stress reduction at radial boundaries. Post-reinforcement with anti-slide piles, landslide-induced thrust on pipelines diminishes. The cross-sectional stress distribution of defective pipelines shows marked changes from multi-peak patterns to single-peak configurations. At landslide centers (model symmetry plane), overall effective stress in pipeline sections decreases dramatically by 304 MPa (59.14% reduction), with effective stress values dropping by 151 MPa (26.87%) for square defects and 114 MPa (20.54%) for ellipsoidal defects. Although the high-stress area at defect locations shrinks significantly compared to un-reinforced conditions, stress discontinuities become more pronounced. The results demonstrate that anti-slide piles can effectively reduce the overall stress on the cross-section of defective gas pipelines, as well as decrease peak stress and the area of high-stress zones at defect locations, which holds significant importance for the protection of defective gas pipelines.

7. Conclusion

To investigate the anti-slide performance of anti-slide piles and their protective effects on gas transmission pipelines, this study employs the strength reduction method and finite element software ABAQUS to establish a numerical model simulating slope impact on pipelines under pile reinforcement. The model enables analysis of pile-soil interaction and evaluates mechanical responses of pipelines under various reinforcement methods. Key findings include:

When the number of anti-slide piles increases, the overall displacement of the landslide mass decreases, with the high-displacement zone shifting from the landslide center (model symmetry plane) to the periphery, ultimately reaching directly above the anti-slide piles. This indicates that the anti-slide effect on slope stabilization intensifies with pile quantity. For gas pipelines, displacement decreases by 168.1mm (a 35.89% reduction year-on-year) as pile count increases. The maximum effective stress of pipelines exhibits a trend of first increasing then decreasing with pile quantity. Notably, pipelines reinforced with a single anti-slide pile demonstrate higher effective stress compared to unreinforced systems, suggesting that insufficient pile quantity may actually increase pipeline failure risks. Therefore, practical engineering projects should maximize anti-slide pile deployment within budget constraints.

When the size of anti-slide piles increases, the maximum displacement of the sliding mass gradually decreases, with particularly significant soil stabilization effects observed directly above the piles and along the landslide perimeter. This demonstrates that larger anti-slide piles substantially enhance slope stabilization performance. For gas pipelines, both displacement and maximum effective stress show marked reductions with increasing pile dimensions, decreasing by 50.28% and 18.82% respectively. The pipeline deformation transitions from plastic deformation to elastic bending. Notably, the effective stress reduction in Scenario 1 compared to Scenario 2 exceeds that in Scenario 2 compared to Scenario 3, indicating the marginal benefits of larger anti-slide piles on pipeline protection capacity become increasingly pronounced. In engineering practice, appropriate pile dimensions should be determined based on actual conditions without excessive enlargement.

The shape of anti-slide piles significantly impacts their slope stabilization effectiveness. While cylindrical anti-slide piles require less construction material than square ones, they demonstrate inferior slope stabilization performance and weaker inherent deformation resistance. For gas pipelines, square anti-slide piles exhibit slightly superior protective effects compared to cylindrical counterparts. No plastic deformation was observed in either configuration, with effective stress and displacement differences measuring 14.3MPa and 5.2mm respectively. These findings indicate negligible differences in protection efficacy between square and cylindrical anti-slide piles for buried gas pipelines. In practical engineering applications, selecting appropriate pile shapes based on topographical conditions and surrounding environmental factors remains the optimal approach.

Further analysis of the defective pipeline reinforced with anti-slide piles reveals that the equivalent plastic strain peak at the center of square defects is significantly higher than that of ellipsoidal defects. The plastic strain zones near both types of defects are markedly reduced compared to the condition without anti-slide piles, with corresponding decreases in equivalent plastic strain peaks. The cross-sectional stress distribution of the defective gas pipeline shows a notable change from the original multi-peak distribution to a single-peak distribution. The overall effective stress at the landslide center of the pipeline decreases significantly under anti-slide

pile reinforcement, with equivalent stress dropping by 26.87% at square defects and 20.54% at ellipsoidal defects. This demonstrates that anti-slide piles effectively reduce both the overall stress level of the defective pipeline's cross-section and peak stress at defect locations, playing a crucial role in ensuring the stable and safe operation of the pipeline.

References

[1] QIAO Xujun. Application of anti-slip piles in landslide treatment engineering [J]. Shanxi Architecture, 2014, 40(33):70-71. DOI: 10.13719/j.cnki.cn14-1279/tu.2014.33.040.

[2] ZENG Jinxiu. Research on slope reinforcement mechanism and calculation theory of slab-connected bundled tendon micro anti-slip pile group [D]. Southwest Jiaotong University, 2019. DOI: 10.27414/d.cnki.gxnju. 2019.003239.

[3] Huang Yongjin. Study on stress mechanism of anti-slip pile support structure of soil-rock composite slope [D]. Chongqing University, 2019.

[4] WANG Long, CHEN Guoxing, HU Wei et al. Stability analysis of unsaturated soil slopes reinforced by anti-slip piles based on quasi-dynamic method [J/OL]. Journal of Disaster Prevention and Mitigation Engineering: 1-8[2023-02-27]. https://doi.org/10.13409/j.cnki.jdpme.20220509005.

[5] Li Ming. Analysis of stress characteristics of steel pipeline crossing soil landslide body and reinforcement of anti-slip pile [D]. Jinan University, 2021. DOI: 10.27166/d.cnki.gsdcc. 2021.000716.

[6] Xin Xing Wu, Ying Fa Lu, Xu Dong Fu. Mechanism and Theoretical Calculations of Buttress Anti-Slide Pile [J]. Advanced Materials Research, 2013, 2331(671-674).

[7] Baoqin Lian, Xingang Wang, Hui Zhong. 3D numerical analysis of anti-slide pile resistance effect and coupling effect of soil-pile interaction [P]. Proceedings of the 4th International Conference on Information Technology and Management Innovation, 2015.

[8] FAN Gang, ZHANG Jian-jing, QI Shun-chao, WU Jin-biao. Dynamic response of a slope reinforced by double-row antisliding piles and pre-stressed anchor cables [J]. Journal of Mountain Science, 2019, 16(01):226-241.

[9] Zhang, Sifeng, Li, Chao, Qi, Hui, Chen, Xingji, Ma, Shuaishuai. Soil Arch Evolution Characteristics and Parametric Analysis of Slope Anchored Anti-slide Pile [J]. KSCE Journal of Civil Engineering, 2021, 25(11).

[10] XU Zhongrui, ZHU Yiwen. Genesis mechanism and stability analysis of landslides in cable-stayed bridges based on displacement inverse analysis method [J]. Science and Technology Bulletin, 2019, 35(11):157-161. DOI: 10.13774/j.cnki.kjtb. 2019.11.031.

[11] Han Chenxi. Numerical simulation study on landslide stability and anti-slip pile treatment in Zhangjiayao under rainfall conditions [D]. Northwest A&F University, 2021. DOI: 10.27409/d.cnki.gxbnu. 2021.000446.

[12] Pan Guoyao. Prevention and monitoring technology of geological disasters in oil and gas pipelines [M]. Beijing: Science Press, 2019.